Platelet activation and aggregation promote lung inflammation and influenza virus pathogenesis

- Vuong Ba Lê, Jochen G. Schneider, Yvonne Boergeling, Fatma Berri, Mariette Ducatez, Jean-Luc Guerin, Iris Adrian, Elisabeth Errazuriz-Cerda, Sonia Frasquilho, Laurent Antunes, et al.

Platelet activation and aggregation promote lung inflammation and influenza virus pathogenesis

Vuong Ba Lê[1*], Jochen G. Schneider[2,3*], Yvonne Boergeling[4], Fatma Berri[1], Mariette Ducatez[5,6], Jean-Luc Guerin[5,6], Iris Adrian[3], Elisabeth Errazuriz-Cerda[7], Sonia Frasquilho[8], Laurent Antunes[8], Bruno Lina[1], Jean-Claude Bordet[9], Martine Jandrot-Perrus[10], Stephan Ludwig[4], Béatrice Riteau[1,9]

[1]EA4610, Lyon, France; [2]Luxembourg Centre for Systems Biomedicine, Esch-Sur-Alzette, Luxembourg; [3]Saarland University Medical Center, Homburg/Saar, Germany; [4]Institute Molecular Virology, ZMBE, Münster, Germany; [5]UMR 1225, IHAP, INRA Toulouse, France; [6]INP, ENVT, Toulouse France; [7]Centre Commun d'Imagerie Quantitative Lyon Est (CIQLE), SFR Santé Lyon-Est, University of Lyon, France.; [8]IBBL, Integrated BioBank of Luxembourg, For Next Generation Healthcare, Luxembourg; [9]Unité d'Hémostase Clinique, Lyon, France; [10]INSERM UMR_S1148, Paris Diderot, CHU Xavier Bichat, Paris, France; [9]INRA Nouzilly, France

* VBL and JGS contributed equally to this work as co–first authors.

Corresponding author: Beatrice Riteau: E-mail: beatrice.riteau@laposte.net.

Author contributions: VBL, JGS, JCB, MJP, SL, and BR designed the experiments. VBL, YB, FB, IA, EEC, SF, and LA performed the experiments. FB, JGS, SL, and BL critically read the manuscript. VBL, MJP and BR wrote the manuscript. **Support:** BR and MJP acquired funding from ANR (ANR-13-BSV3-0011, HemoFlu) and JGS from DFG (SCH682/3-1), EU CIG303682, and FNR CORE Itgb3VascIn. **Short Head:** Platelet dysfunction during influenza; **Classification:** 10.15 Treatment.

Commentary: Our research shows that platelets play a key role in the pathogenesis of influenza-induced acute lung injury. These findings may have an impact on the development of novel drugs for the treatment of these diseases.

Abstract

Rationale: The hallmark of severe influenza virus infections is excessive inflammation of the lungs. Platelets are activated during influenza, but their role in influenza virus pathogenesis and inflammatory responses is unknown.

Objectives: To determine the role of platelets during influenza A virus (IAV) infections and propose new therapeutics against influenza.

Methods: We used targeted gene deletion approaches and pharmacological interventions to investigate the role of platelets during influenza virus infection in mice.

Measurements and Main Results: Lungs of infected mice were massively infiltrated by aggregates of activated platelets. Platelet activation promoted IAV pathogenesis. Activating protease-activated receptor 4 (PAR4), a platelet receptor for thrombin that is crucial for platelet activation, exacerbated influenza-induced acute lung injury and death. In contrast, deficiency in the major platelet receptor glycoprotein IIIa (GPIIIa) protected mice from death caused by influenza viruses, and treating the mice with a specific GPIIbIIIa antagonist, eptifibatide, had the same effect. Interestingly, mice treated with other anti-platelet compounds (antagonists of PAR4, MRS 2179, and clopidogrel) were also protected from severe lung injury and lethal infections induced by several influenza strains.

Conclusions: The intricate relationship between hemostasis and inflammation has major consequences in influenza virus pathogenesis, and anti-platelet drugs might be explored to develop new anti-inflammatory treatment against influenza virus infections.

Key words: Lung injury, novel drugs, Flu pathogenesis, pneumonia, platelets.

Introduction

Influenza is one of the most common infectious diseases in humans, occurring as sporadic pandemic and seasonal epidemic outbreaks, leading to significant numbers of fatalities. Influenza pathogenesis is a complex process involving both viral determinants and the immune system (1-3). During severe influenza, dysregulation of cytokine production contributes to lung damage, possibly leading to organ failure and death (4-6). The endothelium, which lines the interior surface of the blood vessels, is thought to orchestrate the crescendo in cytokine accumulation, although the mechanism involved is not fully understood (7).

Upon endothelial injury, platelets are recruited by inflamed endothelial cells, where they adhere and are activated (8). Simultaneously, the family of protease-activated receptors (PARs) mediates platelet activation by thrombin. PAR4 is strictly required for platelet activation in mice, as mouse platelets do not express PAR1. In contrast, both PAR1 and PAR4 are important for platelet activation in humans. These events lead to a conformational change in the platelet glycoprotein IIb/IIIa (GPIIb/IIIa) receptor for fibrinogen that bridges platelets, leading to their aggregation and a reinforcement of their activation. Importantly, platelet activation is strongly associated with enhanced inflammatory responses. Activated platelets release potent inflammatory molecules and play a key role in leukocyte recruitment (9). Platelet activation is finely tuned, but its dysfunction is pathogenic and contributes to inflammatory disorders (10, 11). Thus, uncontrolled platelet activation could contribute to the pathogenesis of IAV infections by fueling a harmful inflammatory response in the respiratory tract. However, the role of platelets in the context of IAV infection has never been investigated. In the present study, using pharmacological and gene deletion approaches, we

74 investigated the role of platelets in IAV pathogenesis *in vivo*. We found that during severe
75 influenza A virus infection in mice, platelet activation worsens the severity of lung injury.
76

METHODS

Reagents

A549 cells and MDCK cells were purchased from ATCC (Molsheim Cedex, France). IAV A/PR/8/34 virus (H1N1), A/HK/1/68 (H3N2) and A/NL/602/2009 (H1N1) (ATCC) were gifts from G.F. Rimmelzwaan (Erasmus, Netherlands). The highly pathogenic avian A/FPV/Bratislava/79 (H7N7) strain was from the Institute of Molecular Virology, Münster, Germany. The following reagents were used: DAPI (Life Technologies, Paris, France), Alexa Fluor® secondary antibodies (Life Technologies), eptifibatide (Integrilin®, GlaxoSmithKline, Marly-le-Roi, France), Clopidogrel (Santa Cruz Biotechnology, Heidelberg, Germany), MRS 2179 (Tocris Bioscience, Bristol, United Kingdom), PAR4 antagonist pepducin p4pal-10 (Polypeptide Laboratories, Strasbourg, France), PAR4 agonist peptide (AYPGKF-NH_2, Bachem, Weil-am-Rhein, Germany), PAR4 control peptide (YAPGKF-NH2, Bachem) monoclonal anti-neutrophil Ly6G (Cedarlane, Tebu-bio, Le Perray en Yvelines, France), polyclonal anti-platelet CD41 (Bioss, Woburn, USA), monoclonal anti-viral HA (Santa Cruz Biotechnology, Heidelberg, Germany), monoclonal anti-IAV NP (gift from GF. Rimmelzwaan), monoclonal anti-p-Selectin FITC-conjugated (Emfret, Eibelstadt, Germany), monoclonal anti-CD41/61 PE-conjugated (Emfret); Vectastain® ABC kit (Vector Laboratories, Burlingame, USA), 3,3'-diaminobenzidine (DAB) peroxidase substrate (Vector Laboratories), ketamine/xylazine anesthesia (Virbac, Bayer HealthCare, Carros, France), May-Grünwald and Giemsa solutions (Merck, Darmstadt, Germany), hematoxylin and eosin solutions (Diapath, Martinengo, Italy), and enzyme-linked immunosorbent assay (ELISA) kits for mouse IL-6, IL-1β, MIP-2 (PromoCell GmbH, Heidelberg, Germany), IFN-α, IFN-γ, RANTES (R&D Systems, Lille, France), serotonin (BlueGene, Shanghai, China), thromboxane B2 (TXB2; Elabscience, Wuhan, China) and sP-selectin (Qayee-Bio, Shanghai,

China). Total protein was evaluated by using the Coomassie Bradford Protein assay kit (Thermo Scientific, Massachusetts, USA).

Mice

Experiments were performed in accordance with the Guide for the Care and Use of Laboratory Animals of la Direction des Services Vétérinaires (DSV), the French regulations to which our animal care and protocol adhered. The license authority was issued by the DSV and Lyon University (accreditation 78-114). Protocols were approved by the Committee on Ethics of Animal Experiments of Lyon University (Permit BH2008-13).

Female, 7-week-old BALB/c mice were used for H7N7 virus infections. Otherwise, 6-week-old C57BL/6 female mice (Charles River Laboratories, Arbresle, France) and GPIIIa$^{-/-}$ mice or wild-type littermates on a C57BL/6 background were used in this study. For the latter, heterozygous mice were crossed, and WT and KO offspring (males and females) were used. Polymerase chain reaction of tail-tip genomic DNA was performed (12) to determine the absence or presence of the GPIIIa gene. Infection experiments were performed as previously described (13). Mice were anesthetized with ketamine/xylazine (42.5/5 mg/kg) and inoculated intranasally with IAV, in a volume of 20 µl. Eptifibatide was injected intraperitoneally (500 µg/kg or 10 µg/200 µl per mouse of ~20 g body weight) every 3 days until the end of the experiment. MRS 2179 was dissolved in saline buffer and administered once intravenously (50 mg/kg) on day 0. Clopidogrel dissolved in saline buffer was injected intraperitoneally (30 mg/kg) every day until the end of the experiment. For PAR4 stimulation experiments, mice were anesthetized every day for 3 days. On the first day, the anesthetized mice were infected intranasally in the presence or absence of PAR4-AP or control peptide (100 µg/mouse, in a volume of 20 µl). Intranasal peptide treatments were also repeated on days 2 and 3 after

infection. For PAR4 antagonist treatment, pepducin p4pal-10 was given intraperitoneally (0.5 mg/kg) two days post-infection, and treatments were repeated on the next two days.

Upon inoculation, the survival rates were followed. Alternatively, mice were sacrificed at prefixed time points to perform BAL or harvest lungs. ELISA was performed according to the manufacturers' instructions. Virus titers were assessed as previously described (14). Lungs were also harvested for histology and immunohistochemistry as previously described (15).

Evaluation of hemorrhagic foci by histopathological analysis

Lungs from mice inoculated with A/PR/8/34 virus (250 PFU/mouse) with or without eptifibatide treatment were fixed in 10% neutral buffered formalin and embedded in paraffin. Then, 4–6 μm sections were cut and stained with hematoxylin and eosin (H&E) to evaluate histopathological changes. Staining was performed by incubation of the lung sections with Harris hematoxylin for 6 min, running tap water for 1 min, eosin Y for 10 min, 70% ethanol for 1 min, 95% ethanol for 1 min, 100% ethanol for 1 min and two rinses in 100% xylene for 1 min. Histology and injury scoring were performed by a blinded investigator who analyzed the samples and determined the levels of injury according to a semiquantitative scoring system (counting inflammatory infiltration, vascular congestion, hemorrhage, fibrin deposits and epithelial cell apoptosis).

Microscopy

For ultrastructural analysis, lung tissues were cut into 1-mm^3 pieces, fixed in 2% glutaraldehyde at 4°C, washed in 0.2 M cacodylate-HCl buffer containing 0.4 M saccharose and post-fixed in 0.3 M cacodylate-HCl buffer containing 2% osmium tetroxide for 1 hour. After dehydration in a graded alcohol series, tissue samples were impregnated with a 75%

Epon A/25% Epon B/1.7% DMP30 mixture. Tissue embedding entailed polymerization at 60°C for 72 hours. Then, 70-nm sections were cut using an ultramicrotome (Leica Microsystems), mounted on 200-mesh copper grids coated with 1:1,000 polylysine, stabilized for 24 hours and contrasted with uranyl acetate/citrate. Sections were examined using a transmission electron microscope (JEOL 1400, Japan) at 80 kV equipped with an Orius SC600 camera (Gatan, France). Immunogold staining was performed using the anti-HA antibody followed by 10 nm gold-conjugated secondary antibody, as previously described (16). As a control of HA labelling, we used IAV particles that we recently purified (17).

Fluorescence microscopy experiments

Cells from the BAL were centrifuged at 1,800 rpm for 5 minutes at room temperature and suspended in phosphate buffer saline (PBS) at a concentration of $5x10^5$/ml. Then, 100 µl of the solution was used to centrifuge the cells onto coverslips (1,000 rpm for 5 minutes), using a Shandon Cytospin 4 centrifuge. The slides were then dipped in a box containing methanol and kept at -20°C for fixation and permeabilization. After 10 minutes, cells were extensively washed with PBS to remove the fixative. Cells were then incubated with primary antibodies to CD41 and viral HA for 1 hour at room temperature. Revelation was performed using Alexa Fluo® (Life Technologies) secondary antibodies for 1 hour at room temperature. Cells were also counterstained with DAPI for 15 minutes at room temperature. Images were analyzed using a Leica TCS SP5 confocal system (Leica Microsystems).

Evaluation of platelet and leukocyte numbers

Platelets were counted using the Vet ABC™ Hematology Analyzer (SCIL) using the mouse smart card 7030. The automated cell counter differentiates mouse platelets based on their size

176 in multiple sample fluids. Leukocytes and neutrophils in the BAL were visualized by May-
177 Grünwald Giemsa stained cytospin preparations, as previously performed (13).
178
179 **Flow cytometry of blood platelets**
180 Blood was collected in ACD buffer by cardiac puncture. CD41-positive cells and platelet
181 activation in whole blood were evaluated using FITC-conjugated P-selectin and PE-
182 conjugated CD41/CD61 antibodies, as previously described (18, 19).
183
184 **Statistical analysis**
185 The Kaplan-Meier test was used for survival rates. The Mann-Whitney test was used for two-
186 group comparisons of mean percentages in the flow cytometry experiments, lung virus titers,
187 ELISA and total protein quantifications. One-way ANOVA for non-parametric measures
188 (Kruskal-Wallis) was used for multiple-group comparisons in dose-responses or kinetics
189 experiments. Dunn's multiple comparison test was employed as a post hoc test using NI as a
190 control. Probabilities *$p < 0.05$ was considered statistically significant.
191

RESULTS

Platelet recruitment to the lungs upon IAV infection

Platelet recruitment to the lungs was first examined after infection of mice with a sublethal or a 50% lethal dose (LD_{50}) of IAV A/PR/8/34. Immunohistochemistry of the lungs, using monoclonal antibodies for IAV nucleoprotein (NP) and CD41, was used to detect virus-infected cells and platelets, respectively (Figure 1A). At both doses, many IAV-infected cells and marked platelet infiltrates were detected in the lungs of infected mice compared to uninfected mice. To confirm these results, platelet counts in the BAL of infected versus uninfected mice (sublethal dose or LD_{50}) were assessed using a blood cell counter (Figure 1B). In the BAL of infected mice, the platelet levels increased in a dose-dependent manner and were significantly higher than in those of uninfected mice, reaching 50×10^9 cells/L on day 6 post-inoculation (LD_{50}). Differences were not significant upon infection with IAV at the sublethal dose.

Viral proteins are present within platelets

The presence of viral proteins was next determined in platelets from the BAL of infected mice. Platelets were identified by immunofluorescence as CD41 positive, DAPI-negative elements and IAV particles were detected using the viral anti-hemagglutinin (HA) antibody. In contrast to uninfected mice (NI), upon infection (LD_{50}), CD41-positive DAPI-negative platelets stained positively for viral HA, demonstrating that platelets engulfed IAV particles, fragments of IAV or viral proteins *in vivo* (Figure 1C). CD41-negative/DAPI-positive cells were used as controls for antibody specificity. To confirm these results, immunogold labeling of ultrathin cryosections of lungs from uninfected or infected mice was performed using a specific anti-HA antibody. Examination of platelets clearly showed a positive and specific

staining of viral HA proteins, which were located predominantly within platelet granule-like structures (Figure 1D, middle and upper right panels). The sparse staining could have been due to the procedure. Indeed, as a control, we used immunogold labelling of HA on highly purified A/PR/8/34 virus particles (17). Although virions of IAV contain approximatively 500 molecules of HA per virion, few gold particles were observed (Figure 1D, lower right panel).

Platelet activation and aggregation

Upon activation, platelets become immobilized, secrete their granule content, and aggregate. Serotonin is released from platelet dense granules, and P-selectin is rapidly translocated from the alpha granules to the plasma membrane and shed. Thus, we next analyzed these responses in the lungs of infected mice (sublethal or LD_{50}). Serotonin and soluble P-selectin (sP-selectin) were measured in BAL and plasma, respectively, by ELISA (Figure 2A). Serotonin and sP-selectin were significantly higher in the fluid of infected mice compared to uninfected mice. Significant differences were only observed upon infection with IAV at LD_{50}. Furthermore, exposure of P-selectin on the surface of platelets isolated from IAV-infected mice was increased compared to uninfected mice (Figure 2B, left panel). The average percentage of P-selectin-positive platelets reached 23% upon infection, versus 5% in uninfected mice (Figure 2B, right panel). Moreover, transmission electron microscopy showed that platelets in the lungs of influenza virus-infected mice were tightly packed, forming large extravascular aggregates with signs of shape change and some platelets were devoid of granules (Figure 2C). In contrast, in the lungs of uninfected mice, only a few isolated platelets were detected.

Platelets contribute to influenza pathogenesis

Platelet GPIIIa$^{+/-}$ mice were intercrossed to generate wild-type (WT) and platelet GPIIIa$^{-/-}$ mice, which were then infected with IAV A/PR/8/34, and the survival rates were monitored. As shown in Figure 2D, compared to WT mice, GPIIIa$^{-/-}$ mice were significantly more resistant to IAV-induced death.

Time course of platelet activation, IL1-β release and platelet binding to leukocytes

Platelets were counted in the BAL of infected mice (LD_{50}) at various times post-inoculation. Upon infection, platelet counts increased in a time-dependent manner (Figure 3A), peaked on day 3 and stayed elevated until day 8. Plasmatic sP-selectin significantly increased during the course of infection and plateaued on days 3-8 (Figure 3B). Increased IL1-β was also detected in the BAL and blood of infected mice but with different lags (Figure 3C-D). IL1-β was released in the BAL paralleled platelet activation, whereas IL1-β peaked in the blood on day 2 post-inoculation and then rapidly decreased. Ultrastructural analysis of the lungs of A/PR/8/34-infected mice showed that platelet-leukocyte complexes formed *in vivo*. Neutrophils and monocytes were associated with platelet aggregates, although not all platelets adhered to leukocytes (Figure 3E).

PAR4 promotes pathogenesis of IAV infection in a platelet-dependent pathway

Mice were inoculated with a sublethal dose of IAV A/PR/8/34 and stimulated with 100 µg/mouse of the PAR4 agonist peptide AYPGKF-NH_2 (PAR4-AP) or the inactive control peptide YAPGKF-NH_2 (Control-P). As expected, the content of serotonin and sP-selectin was increased in the BAL of infected mice treated with PAR4-AP compared to Control-P, indicating an increased level of platelet activation (Figure 4A). More interestingly, upon infection, mice treated with PAR4-AP displayed significantly higher mortality rates compared with mice treated with Control-P (Figure 4B). In contrast, treatment with PAR4-AP did not

affect the survival of uninfected mice. The effect was platelet dependent, as treatment of mice with eptifibatide, an antagonist of the GPIIbIIIa platelet receptor, abrogated the deleterious effect of PAR4-AP (Figure 4C), as did the platelet GPIIIa deficiency (Figure 4D). This indicated that PAR4-AP-induced platelet aggregation increased the severity of the IAV symptoms. No significant differences in lung virus titer were observed 3 or 6 days post-inoculation between mice treated with PAR4-AP and those treated with Control-P (Figure 4E). However, on day 6, treatment with PAR4-AP significantly increased total proteins in the BAL (Figure 4F). The response levels of IL-6, IL-1β and MIP-2 were also enhanced, while those of interferon (IFN)-γ, RANTES and KC were unaffected (Figure 5A). On day 3, no difference was observed. Thus, PAR4 activation promoted IAV-induced inflammation of the lungs at later time points post-infection. Similarly, staining of lung sections on day 6 revealed marked cellular infiltrates of leukocytes (HE) and neutrophils (Ly6G) in the lungs of PAR4-AP-treated mice compared to controls (Figure 5B). Similar numbers of IAV-infected cells were detected by immunohistochemistry using an anti-NP antibody. No staining was observed in the lungs of uninfected control mice.

PAR4 antagonism protects against influenza virus pathogenicity

When mice were infected with IAV A/PR/8/34 (LD_{50}), treatment with pepducin p4pal-10 protected them from death (Figure 6A). Substantial protection was also observed against infection with an H3N2 virus, A/HK/1/68. The protection conferred by PAR4 antagonism correlated with the degree of inhibition of platelet activation. In the BAL of pepducin p4pal-10-treated mice, decreased thromboxane B2 (TXB2), a specific marker of platelet activation, was observed (Figure 6B). In contrast, no difference in the mean lung virus titers was detected on day 3 or 6 after inoculation with IAV A/PR/8/34 (Figure 6C). However, treatment with pepducin p4pal-10 significantly reduced the recruitment of leukocytes (Figure 6D), including

neutrophils, in BAL on day 6. Total proteins (Figure 6E) and IL-6, IL-1β and MIP-2 (Figure 6F) were also decreased. Consistent with those results, histopathology revealed that treatment with pepducin p4pal-10 reduced infiltration of inflammatory cells (HE), including neutrophils (Ly6G), in the lungs of infected mice (Figure 6G), while similar numbers of IAV-infected cells (NP) were detected by immunohistochemistry.

The anti-platelet drug eptifibatide protects mice from lethal influenza infection

Mice were inoculated with IAV A/PR/8/34 (LD_{50}) and were treated or not with 500 µg/kg of eptifibatide every 3 days. This dosage is comparable to the lowest doses used clinically in humans (20-22). Eptifibatide treatment had a dramatic effect on lung infiltration by platelets: platelet aggregation was totally prevented, and only isolated platelets were observed (Figure 7A). Furthermore, this effect was accompanied by decreases in TXB2 and sP-selectin in the fluid of infected mice compared to controls (Figure 7B), showing that inhibition of platelet aggregation also limited the extent of platelet activation. More importantly, treatment with eptifibatide improved the outcome of infection with A/PR/8/34 virus and prevented mortality of the mice (Figure 7C). Protection was also observed with other influenza strains. No effect of eptifibatide was observed in $GPIIIa^{-/-}$ mice (Figure 8A), showing the specificity of the drug.

The protective effect of eptifibatide was independent of virus replication in lungs (Figure 8B) and IFN-α release in the BAL (Figure 8C). In contrast, it was correlated with decreased total proteins and levels of certain cytokines in the BAL of eptifibatide-treated mice (Figure 8D-E). Immunohistochemistry confirmed that treatment by eptifibatide prevented IAV-induced lung alveolar damage (HE) and neutrophil infiltration (Ly6G) but not viral replication (NP) on day 6 post-infection (Figure 8F). This effect was not observed on day 2 (data not shown).

315 Treatment of infected mice with MRS 2179 and clopidogrel, which inhibits the ADP
316 receptors P2Y1 and P2Y12, improved the outcome of IAV infection (Figure 8G).
317
318 **Eptifibatide treatment protects mice from lung injury induced by influenza**
319 Histopathological analyses of lung tissues were performed to evaluate the extent of
320 hemorrhage after eptifibatide treatment. Mice were infected with A/PR/8/34 virus and treated
321 with eptifibatide or vehicle, and lungs were then harvested 6 days post-inoculation for
322 histopathology. In the infected group, lungs presented signs of congestion with infiltration of
323 neutrophils and monocytes, interstitial and alveolar hemorrhages, as well as thrombosis
324 (Figure 9A). Fibrin and erythrocyte-rich thrombi were observed in small vessels. Figure 9B
325 summarizes the blinded semi-quantitative scoring of the different parameters. Eptifibatide
326 markedly reduced the severity of pulmonary injury induced by influenza virus infections, and
327 a marked reduction in neutrophil infiltration was observed. (Figure 9A-B). More importantly,
328 almost no hemorrhage was detected in the lungs of infected mice treated with eptifibatide.
329

DISCUSSION

The present study shows that platelets play an active role in fueling the dysregulation of inflammation and promoting pathogenesis of influenza virus infections. Histological analysis of lungs provided evidence that platelets massively infiltrate the lungs of infected mice. Additionally, infiltrated platelets stained positive for viral HA, based on immunofluorescence staining of BAL and immunogold labeling of ultrathin cryosections of lungs. The technical limitation of the staining did not allow us to determine whether platelets engulfed the entire virions, only IAV fragments or antigens. However, because platelets incorporate influenza viruses *in vitro* (23), our results suggest that platelets recruited to the lungs most likely take up IAV particles *in vivo* as well. This could consist of a passive passage of particles through the open canalicular system, the tortuous invaginations of platelet surface membranes tunneling through the cytoplasm, in a manner similar to bacterial ingestion (24). Alternatively, uptake of IAVs may be compared to phagocytosis by macrophages and neutrophils, as previously observed for human immunodeficiency viruses (25).

Ultrastructural analysis showed that features of platelets in the lungs of infected mice are those of aggregates of activated platelets: platelets were tightly stacked without interplatelet spaces, and some platelets were devoid of granules, suggesting that they had degranulated. Consistent with those observations, markers of platelet activation were detected in the BAL and plasma of infected mice. Thus, upon lethal IAV infection, platelets are activated in the lung and in the peripheral circulation. Our observations are consistent with the recent findings that influenza virus activates platelets through FcγRIIA signaling or thrombin generation (26). Also, thrombin triggers the release of serotonin and TXA2 from platelets, promotes P-selectin translocation to the platelet plasma membrane and activates the GPIIb/IIIa complex (27).

Platelets contribute to the host defense against bacterial infectious agents by limiting vascular lesions and inducing injury repair (28, 29). However, unbalanced platelet activation may have pathological consequences. In the IAV infection model used in this study, platelet activation and aggregation proved to be deleterious. PAR4 and GPIIIa are both key molecules in platelet function. PAR4 is strictly required for platelet activation in mice, while GPIIIa is required for platelet aggregation. First, mice deficient in GPIIIa were protected from lung injury and death. Furthermore, stimulation of PAR4 increased lung inflammation and the severity of IAV infection. In contrast, PAR4 antagonists protected mice from death. Our results indicate that PAR4 acts through platelet activation because the effect of PAR4-AP was abrogated when infected mice were treated with the platelet specific inhibitor eptifibatide (30), or when mice were deficient in platelet GPIIIa protein. Altogether, the data indicate that platelets regulate IAV pathogenesis.

Interestingly, the observation by others that influenza virus activates platelets through thrombin generation (26) suggests that thrombin may also act in a deleterious manner against IAV infection. Thrombin mediates signal transduction mainly by activating PAR4 and PAR1 (31, 32). Because mouse platelets do not express PAR1, thrombin-mediated platelet activation most likely occurs through PAR4 activation, but thrombin activation of PAR1 may also be involved in the pathogenesis of IAV infection. Indeed, we recently found that PAR1 signaling contributes to IAV pathogenicity in mice (33). In this context, PAR1 cooperates with plasminogen, which controls pathogenesis, via fibrinolysis (34). Thus, investigations into the role of hemostasis dysregulation may help better understand IAV pathogenesis (35-37).

In several models of injury, uncontrolled platelet activation drives deleterious inflammation (38). Activated platelets release an arsenal of potent pro-inflammatory molecules (39), which exacerbate neutrophil rolling, adhesion and recruitment (40-42). In addition, the physical interaction between platelets and neutrophils further contributes to neutrophil retention and activation (42). Because dysregulation of inflammation is a hallmark of severe influenza virus infections, it is likely that platelets have a pro-inflammatory effect with a key role in IAV pathogenesis. In our study, electron microscopy demonstrated the presence of neutrophil-platelet complexes upon IAV infection. The anti-platelet molecule eptifibatide inhibited neutrophil recruitment into inflamed lungs (Figure 9). Thus, platelet interaction with neutrophils is likely to play a role during severe inflammation induced by influenza.

Interestingly, the exacerbation of cytokine production induced by platelet activation was only observed at later time points after infection. Upon infection, the virus is recognized as foreign by highly conserved receptors known as pattern recognition receptors. Activation of these receptors results in the secretion of cytokines and chemokines, which corresponds to the early inflammatory response against IAV infection (35). Thus, the amplification and intensity of inflammation depends on the replicative capacity of the virus. When the response is tightly controlled, a resolution phase of inflammation is engaged at later time points post-infection, and this partly determines the duration of inflammation. Resolution of inflammation is largely influenced by the vascular endothelium (43). Upon injury of the latter, platelets are activated. Our data show coordinated platelet activation/aggregation and inflammatory responses at late time points post-infection, indicating that platelets may affect the recovery phase after infection and wound healing. In this scenario, extravasation of large numbers of platelets and leukocytes would be the basis of the defect in the resolution phase of the inflammation. Most

likely, this further promotes hemostasis dysregulation, such as fibrinolysis (18, 44) or PAR1 activation (33, 45), fueling the vicious circle of inflammation (34, 35).

Recurrent outbreaks of IAV that cause severe infections in humans have raised serious concerns about therapeutic strategies available for these pathogens. Current treatments that target viral proteins have a number of disadvantages, including the rapid development of resistant virus variants as a result of selective pressure (46, 47). Because targeting the host rather than the virus would not easily lead to resistance, drugs regulating inflammation are appealing as potential new therapeutics for IAV symptoms (13, 33, 34, 48). Here, we found that available anti-platelet drugs efficiently protected mice from IAV pathogenesis induced by several influenza strains. These results are consistent with other studies showing that aspirin, known to inhibit platelet activation, blocks IAV propagation via NF-kB inhibition (49). Altogether, these results suggest that anti-platelet drugs might be explored as new anti-inflammatory treatments against severe influenza.

ACKNOWLEDGMENTS

Authors are grateful to Dr. P. Clézardin (Inserm UMR S1033, France) and Dr. C. Dumontet (Cancer Center of Lyon, France) for help with the immunohistochemistry and immunofluorescence. Our study received only governmental funding. No pharmaceutical industries have been involved in this study.

425

426 **REFERENCES**

427

428 1. Kuiken T, Riteau B, Fouchier RA, Rimmelzwaan GF. Pathogenesis of influenza virus
429 infections: The good, the bad and the ugly. *Curr Opin Virol* 2012;2:276-286.
430 2. Fukuyama S, Kawaoka Y. The pathogenesis of influenza virus infections: The
431 contributions of virus and host factors. *Current opinion in immunology* 2011;23:481-486.
432 3. Foucault ML, Moules V, Rosa-Calatrava M, Riteau B. Role for proteases and hla-g in
433 the pathogenicity of influenza a viruses. *J Clin Virol* 2011;51:155-159.
434 4. Cheung CY, Poon LL, Lau AS, Luk W, Lau YL, Shortridge KF, Gordon S, Guan Y,
435 Peiris JS. Induction of proinflammatory cytokines in human macrophages by influenza a
436 (h5n1) viruses: A mechanism for the unusual severity of human disease? *Lancet*
437 2002;360:1831-1837.
438 5. de Jong MD, Simmons CP, Thanh TT, Hien VM, Smith GJ, Chau TN, Hoang DM,
439 Chau NV, Khanh TH, Dong VC, Qui PT, Cam BV, Ha do Q, Guan Y, Peiris JS, Chinh NT,
440 Hien TT, Farrar J. Fatal outcome of human influenza a (h5n1) is associated with high viral
441 load and hypercytokinemia. *Nature medicine* 2006;12:1203-1207.
442 6. Kobasa D, Jones SM, Shinya K, Kash JC, Copps J, Ebihara H, Hatta Y, Kim JH,
443 Halfmann P, Hatta M, Feldmann F, Alimonti JB, Fernando L, Li Y, Katze MG, Feldmann H,
444 Kawaoka Y. Aberrant innate immune response in lethal infection of macaques with the 1918
445 influenza virus. *Nature* 2007;445:319-323.
446 7. Teijaro JR, Walsh KB, Cahalan S, Fremgen DM, Roberts E, Scott F, Martinborough
447 E, Peach R, Oldstone MB, Rosen H. Endothelial cells are central orchestrators of cytokine
448 amplification during influenza virus infection. *Cell* 2011;146:980-991.

449 8. Rumbaut RE, Thiagarajan P. Platelet-vessel wall interactions in hemostasis and
450 thrombosis. San Rafael (CA); 2010.
451 9. Duerschmied D, Suidan GL, Demers M, Herr N, Carbo C, Brill A, Cifuni SM, Mauler
452 M, Cicko S, Bader M, Idzko M, Bode C, Wagner DD. Platelet serotonin promotes the
453 recruitment of neutrophils to sites of acute inflammation in mice. *Blood* 2013;121:1008-1015.
454 10. Cohen J. The immunopathogenesis of sepsis. *Nature* 2002;420:885-891.
455 11. Degen JL, Bugge TH, Goguen JD. Fibrin and fibrinolysis in infection and host
456 defense. *J Thromb Haemost* 2007;5 Suppl 1:24-31.
457 12. Riteau B, Moreau P, Menier C, Khalil-Daher I, Khosrotehrani K, Bras-Goncalves R,
458 Paul P, Dausset J, Rouas-Freiss N, Carosella ED. Characterization of hla-g1, -g2, -g3, and -g4
459 isoforms transfected in a human melanoma cell line. *Transplant Proc* 2001;33:2360-2364.
460 13. Khoufache K, LeBouder F, Morello E, Laurent F, Riffault S, Andrade-Gordon P,
461 Boullier S, Rousset P, Vergnolle N, Riteau B. Protective role for protease-activated receptor-2
462 against influenza virus pathogenesis via an ifn-gamma-dependent pathway. *J Immunol*
463 2009;182:7795-7802.
464 14. Riteau B, de Vaureix C, Lefevre F. Trypsin increases pseudorabies virus production
465 through activation of the erk signalling pathway. *J Gen Virol* 2006;87:1109-1112.
466 15. Riteau B, Faure F, Menier C, Viel S, Carosella ED, Amigorena S, Rouas-Freiss N.
467 Exosomes bearing hla-g are released by melanoma cells. *Hum Immunol* 2003;64:1064-1072.
468 16. LeBouder F, Morello E, Rimmelzwaan GF, Bosse F, Pechoux C, Delmas B, Riteau B.
469 Annexin ii incorporated into influenza virus particles supports virus replication by converting
470 plasminogen into plasmin. *J Virol* 2008;82:6820-6828.
471 17. Berri F, Haffar G, Le VB, Sadewasser A, Paki K, Lina B, Wolff T, Riteau B. Annexin
472 v incorporated into influenza virus particles inhibits gamma interferon signaling and promotes
473 viral replication. *J Virol* 2014;88:11215-11228.

18. LeBouder F, Lina B, Rimmelzwaan GF, Riteau B. Plasminogen promotes influenza a virus replication through an annexin 2-dependent pathway in the absence of neuraminidase. *J Gen Virol* 2010;91:2753-2761.

19. LeBouder F, Khoufache K, Menier C, Mandouri Y, Keffous M, Lejal N, Krawice-Radanne I, Carosella ED, Rouas-Freiss N, Riteau B. Immunosuppressive hla-g molecule is upregulated in alveolar epithelial cells after influenza a virus infection. *Hum Immunol* 2009;70:1016-1019.

20. Hassan W, Al-Sergani H, Al Buraiki J, Dunn B, Al Turki F, Akhras N, Elshaer F, Nawaz M, Kharabsheh S, ElKum N. Immediate and intermediate results of intracoronary stand-alone bolus administration of eptifibatide during coronary intervention (ice) study. *American heart journal* 2007;154:345-351.

21. Gilchrist IC, O'Shea JC, Kosoglou T, Jennings LK, Lorenz TJ, Kitt MM, Kleiman NS, Talley D, Aguirre F, Davidson C, Runyon J, Tcheng JE. Pharmacodynamics and pharmacokinetics of higher-dose, double-bolus eptifibatide in percutaneous coronary intervention. *Circulation* 2001;104:406-411.

22. Tcheng JE, Talley JD, O'Shea JC, Gilchrist IC, Kleiman NS, Grines CL, Davidson CJ, Lincoff AM, Califf RM, Jennings LK, Kitt MM, Lorenz TJ. Clinical pharmacology of higher dose eptifibatide in percutaneous coronary intervention (the pride study). *The American journal of cardiology* 2001;88:1097-1102.

23. Danon D, Jerushalmy Z, De Vries A. Incorporation of influenza virus in human blood platelets in vitro. Electron microscopical observation. *Virology* 1959;9:719-722.

24. White JG. Platelets are covercytes, not phagocytes: Uptake of bacteria involves channels of the open canalicular system. *Platelets* 2005;16:121-131.

497 25. Youssefian T, Drouin A, Masse JM, Guichard J, Cramer EM. Host defense role of
498 platelets: Engulfment of hiv and staphylococcus aureus occurs in a specific subcellular
499 compartment and is enhanced by platelet activation. *Blood* 2002;99:4021-4029.
500 26. Boilard E, Pare G, Rousseau M, Cloutier N, Dubuc I, Levesque T, Borgeat P, Flamand
501 L. Influenza virus h1n1 activates platelets through fcgammariia signaling and thrombin
502 generation. *Blood* 2014;123:2854-2863.
503 27. Polley MJ, Leung LL, Clark FY, Nachman RL. Thrombin-induced platelet membrane
504 glycoprotein iib and iiia complex formation. An electron microscope study. *J Exp Med*
505 1981;154:1058-1068.
506 28. Petaja J. Inflammation and coagulation. An overview. *Thromb Res* 2011;127 Suppl
507 2:S34-37.
508 29. Engelmann B, Massberg S. Thrombosis as an intravascular effector of innate
509 immunity. *Nat Rev Immunol* 2013;13:34-45.
510 30. Tardiff BE, Jennings LK, Harrington RA, Gretler D, Potthoff RF, Vorchheimer DA,
511 Eisenberg PR, Lincoff AM, Labinaz M, Joseph DM, McDougal MF, Kleiman NS,
512 Investigators P. Pharmacodynamics and pharmacokinetics of eptifibatide in patients with
513 acute coronary syndromes: Prospective analysis from pursuit. *Circulation* 2001;104:399-405.
514 31. Kahn ML, Nakanishi-Matsui M, Shapiro MJ, Ishihara H, Coughlin SR. Protease-
515 activated receptors 1 and 4 mediate activation of human platelets by thrombin. *J Clin Invest*
516 1999;103:879-887.
517 32. Kataoka H, Hamilton JR, McKemy DD, Camerer E, Zheng YW, Cheng A, Griffin C,
518 Coughlin SR. Protease-activated receptors 1 and 4 mediate thrombin signaling in endothelial
519 cells. *Blood* 2003;102:3224-3231.

520 33. Khoufache K, Berri F, Nacken W, Vogel AB, Delenne M, Camerer E, Coughlin SR,
521 Carmeliet P, Lina B, Rimmelzwaan GF, Planz O, Ludwig S, Riteau B. Par1 contributes to
522 influenza a virus pathogenicity in mice. *J Clin Invest* 2013;123:206-214.
523 34. Berri F, Rimmelzwaan GF, Hanss M, Albina E, Foucault-Grunenwald ML, Le VB,
524 Vogelzang-van Trierum SE, Gil P, Camerer E, Martinez D, Lina B, Lijnen R, Carmeliet P,
525 Riteau B. Plasminogen controls inflammation and pathogenesis of influenza virus infections
526 via fibrinolysis. *PLoS Pathog* 2013;9:e1003229.
527 35. Berri F, Le VB, Jandrot-Perrus M, Lina B, Riteau B. Switch from protective to
528 adverse inflammation during influenza: Viral determinants and hemostasis are caught as
529 culprits. *Cellular and molecular life sciences : CMLS* 2014;71:885-898.
530 36. Antoniak S, Mackman N. Multiple roles of the coagulation protease cascade during
531 virus infection. *Blood* 2014;123:2605-2613.
532 37. Pryzdial EL, Sutherland MR, Ruf W. The procoagulant envelope virus surface:
533 Contribution to enhanced infection. *Thromb Res* 2014;133 Suppl 1:S15-17.
534 38. Henn V, Slupsky JR, Grafe M, Anagnostopoulos I, Forster R, Muller-Berghaus G,
535 Kroczek RA. Cd40 ligand on activated platelets triggers an inflammatory reaction of
536 endothelial cells. *Nature* 1998;391:591-594.
537 39. von Hundelshausen P, Weber KS, Huo Y, Proudfoot AE, Nelson PJ, Ley K, Weber C.
538 Rantes deposition by platelets triggers monocyte arrest on inflamed and atherosclerotic
539 endothelium. *Circulation* 2001;103:1772-1777.
540 40. Diacovo TG, Roth SJ, Buccola JM, Bainton DF, Springer TA. Neutrophil rolling,
541 arrest, and transmigration across activated, surface-adherent platelets via sequential action of
542 p-selectin and the beta 2-integrin cd11b/cd18. *Blood* 1996;88:146-157.

543 41. Mayadas TN, Johnson RC, Rayburn H, Hynes RO, Wagner DD. Leukocyte rolling
544 and extravasation are severely compromised in p selectin-deficient mice. *Cell* 1993;74:541-
545 554.
546 42. Zarbock A, Polanowska-Grabowska RK, Ley K. Platelet-neutrophil-interactions:
547 Linking hemostasis and inflammation. *Blood reviews* 2007;21:99-111.
548 43. Kadl A, Leitinger N. The role of endothelial cells in the resolution of acute
549 inflammation. *Antioxidants & redox signaling* 2005;7:1744-1754.
550 44. Berri F, Le VB, Jandrot-Perrus M, Lina B, Riteau B. Switch from protective to
551 adverse inflammation during influenza: Viral determinants and hemostasis are caught as
552 culprits. *Cellular and molecular life sciences : CMLS* 2013.
553 45. Aerts L HM, Rhéaume C, Lavigne S, Couture C, Kim W, Susan-Resiga D, Prat A,
554 Seidah NG,Vergnolle N , Riteau B, Boivin G. Modulation of protease activated receptor 1
555 influences human metapneumovirus disease severity in a mouse model. *Plos One*
556 2013;28;8(8):e72529.
557 46. Song MS, Hee Baek Y, Kim EH, Park SJ, Kim S, Lim GJ, Kwon HI, Pascua PN,
558 Decano AG, Lee BJ, Kim YI, Webby RJ, Choi YK. Increased virulence of neuraminidase
559 inhibitor-resistant pandemic h1n1 virus in mice: Potential emergence of drug-resistant and
560 virulent variants. *Virulence* 2013;4:489-493.
561 47. Butler J, Hooper KA, Petrie S, Lee R, Maurer-Stroh S, Reh L, Guarnaccia T, Baas C,
562 Xue L, Vitesnik S, Leang SK, McVernon J, Kelso A, Barr IG, McCaw JM, Bloom JD, Hurt
563 AC. Estimating the fitness advantage conferred by permissive neuraminidase mutations in
564 recent oseltamivir-resistant a(h1n1)pdm09 influenza viruses. *PLoS Pathog*
565 2014;10:e1004065.
566 48. Walsh KB, Teijaro JR, Wilker PR, Jatzek A, Fremgen DM, Das SC, Watanabe T,
567 Hatta M, Shinya K, Suresh M, Kawaoka Y, Rosen H, Oldstone MB. Suppression of cytokine

storm with a sphingosine analog provides protection against pathogenic influenza virus. *Proc Natl Acad Sci U S A* 2011;108:12018-12023.

49. Mazur I, Wurzer WJ, Ehrhardt C, Pleschka S, Puthavathana P, Silberzahn T, Wolff T, Planz O, Ludwig S. Acetylsalicylic acid (asa) blocks influenza virus propagation via its nf-kappab-inhibiting activity. *Cell Microbiol* 2007;9:1683-1694.

FIGURE LEGENDS

Figure 1: Upon IAV infection, platelets infiltrate the lungs, and IAV particles are observed in platelets. (A) Immunohistochemistry analysis of lungs from uninfected (NI) or infected mice inoculated with A/PR/8/34 virus, at a sublethal dose (75 pfu/mouse) or LD_{50} (250 pfu/mouse; day 6 post-infection). Antibodies against the IAV nucleoprotein (NP) and CD41 were used to detect virus infected cells and platelets, respectively. The results are representative of three mice per group. (B) Platelet numbers in BAL were assessed using a Vet ABC™ Hematology Analyzer on day 6 post-inoculation of mock or IAV-infected mice. Data are presented as the means ± SEM of 4 mice per group, ** $p<0.01$ for LD_{50} vs. NI. (C) Immunofluorescence staining of viral particles in platelets from BAL was performed with anti-influenza HA antibody. Platelets were detected with anti-CD41 antibody, and nuclei were counterstained with DAPI. The merged images are shown on the right panel. CD41-negative cells from BAL were used as a negative control. (D) Immunogold labeling of ultrathin cryosections of lungs of uninfected (NI) or A/PR/8/34 virus-infected mice (LD_{50}, 250 pfu/mouse, day 6 post-infection) was performed using a specific anti-HA antibody. Black arrows indicate viral particles. Staining of a platelet-granule like structure is shown on the upper right panel. As a control for HA staining, electron microscopic immunogold labeling was performed on purified A/PR/8/34 viruses using the anti-HA antibody (lower right panel).

Figure 2: Upon IAV infection, platelets are stimulated and contribute to influenza pathogenesis. (A) Serotonin and sP-selectin were measured by ELISA in the BAL and plasma of Mock (NI) or A/PR/8/34 virus-infected mice, respectively, on day 6 post-inoculation (75 pfu/mouse, sublethal dose or 250 pfu/mouse, LD_{50}). Data represent the means ± SEM of 4 mice per group, * $p<0.05$ for LD_{50} vs. NI; ** $p<0.01$ for LD_{50} vs. NI. (B) Blood

samples from uninfected (NI) or infected mice were double-stained with anti-P-selectin and anti-CD41 antibody as a platelet identifier. The mean percentage ± SEM of activated platelets (CD41 and P-selectin-positive) from five mice per group is shown in the right panel, * $p<0.05$ for LD_{50} vs. NI. (C) Ultrastructure analysis of platelets in the lungs of uninfected and infected mice (A/PR/8/34, 250 pfu/mouse, LD_{50}). Note the aggregation of platelets in the lungs of infected mice along with their morphological changes (arrows) and the absence of granules in some of them, which reflects their degranulation (asterisks). Sections show platelet aggregates with an interstitial localization. (D) Survival of platelet $GPIIIa^{-/-}$ mice and WT littermates after infection with A/PR/8/34 virus at a LD_{50} (250 pfu/mouse, n=9-10 mice per group) or lethal dose (350 pfu/mouse n=6 mice per group); * $p<0.05$ and ** $p<0.01$, respectively.

Figure 3: Platelet activation and inflammation. (A) Platelet numbers in BAL of A/PR/8/34 virus infected mice (250 pfu/mouse, LD_{50}) were assessed using a Vet ABC™ Hematology Analyzer, at the indicated time post-inoculation. The results are represented as the means ± SEM of 4 mice per group. On days 0 and 6, additional results from Figure 1B are included. (B-D) sP-selectin in the plasma (B), IL1-β in the BAL (C) and IL1-β in the plasma (D) of infected mice (A/PR/8/34, 250 pfu/mouse, LD_{50}) were determined by ELISA at the indicated times. The results from panels B-D represent the means ± SEM of 4 mice per group. From A-D: * $p<0.05$, ** $p<0.01$, *** $p<0.001$ for the indicated time vs. 0. (E) Ultrastructural analysis of platelets associated with leukocytes in the lungs of infected mice (A/PR/8/34, 250 pfu/mouse, LD_{50}). The star shows platelet aggregates that are not adherent to leukocytes.

Figure 4: Effects of PAR4 activation on IAV pathogenicity, virus replication and inflammation. (A) Serotonin and sP-selectin were measured by ELISA in the BAL and plasma, respectively, of infected mice (A/PR/8/34, 75 pfu/mouse, sublethal dose) after

627 treatment with PAR4-AP or control peptide (Control-P) on day 6 post-inoculation. Columns
628 represent the means ± SEM (n=4-5). ** p<0.01; * p<0.05. (B) Time course of IAV-induced
629 death in mice in response to PAR4 stimulation. Mice were mock-infected or inoculated with
630 A/PR/8/34virus (75 pfu/mouse, sublethal dose, n=18-19 mice per group; or 250 pfu/mouse,
631 LD_{50}, n=6-12 mice per group) and treated with either control peptide or PAR4-AP. * p<0.05;
632 ** p<0.01. (C) Time course of IAV-induced death in mice (A/PR/8/34virus) in response to
633 PAR4 stimulation and after treatment or no treatment with eptifibatide (n=6-18 mice per
634 group). * p<0.05 for PAR4-AP vs. control-P. A significant difference (p<0.01) was also found
635 between groups treated with PAR-AP ± eptifibatide (not shown) (D) Time course of IAV-
636 induced death in WT (n=10 mice per group) and $GPIIIa^{-/-}$ mice (n=7-9 mice per group) in
637 response to PAR4 stimulation (A/PR/8/34virus). The same mice were used in Figure 2D (250
638 pfu/mouse, dose LD_{50}). *** p<0.001 for PAR4-AP vs. control-P in WT mice. (E) Lung virus
639 titers after infection of mice with A/PR/8/34 virus (sublethal dose) stimulated or not with
640 PAR4-AP. (F) Total protein quantification in BAL of infected mice in response to PAR4
641 stimulation. For E and F, the results represent the means ± SEM (n=3-5). ** p<0.01 for
642 PAR4-AP vs. control-P.
643
644 **Figure 5: PAR4-AP increases lung inflammation upon A/PR/8/34 virus infection.** (A)
645 Cytokines in the BAL of infected mice (75 pfu/mouse, sublethal dose), treated with PAR4-AP
646 or control peptide, were measured by ELISA 3 and 6 days after inoculation. Uninfected mice
647 (NI) were used as control. The results represent the means ± SEM (n=3-5). * p<0.05, **
648 p<0.01 for PAR4-AP vs. control-P. (B) Histopathological analysis of lungs from uninfected
649 mice or mice infected with a sublethal dose (75 pfu/mouse) of A/PR/8/34 virus after treatment
650 with PAR4-AP or control peptide, on day 6 post-infection. Thin sections of lungs were
651 stained with hematoxylin and eosin (HE). Note the marked infiltration of cells in the lungs of

infected mice stimulated with PAR4-AP. Immunohistochemistry used antibodies against Ly6G. Viral NP was used to detect neutrophils and virus-infected cells. Data are representative of three mice per group.

Figure 6: PAR4 antagonist protects mice against IAV infection and deleterious lung inflammation. (A) IAV-induced pathogenesis in mice treated or not with the PAR4 antagonist pepducin p4pal-10 (pepducin). Mice were inoculated with A/PR/8/34 virus (250 pfu/mouse, LD_{50}, n=13 mice per group) or A/HK/1/68 (100 pfu/mouse, LD_{50}, n=12 mice per group) and treated with pepducin or saline. Survival was then monitored for 2 weeks. * $p<0.05$. (B) Thromboxane B2 (TXB2) was measured by ELISA in the BAL of infected mice (A/PR/8/34, 250 pfu/mouse, LD_{50}) after treatment with pepducin or vehicle, on day 6 post-inoculation. Data represent the mean ± SEM of 4-6 mice per group. (C) Lung virus titers after infection of mice with A/PR/8/34 virus (250 pfu/mouse, LD_{50}) treated with pepducin or vehicle. The results represent the means ± SEM from 3 individual animals per group. (D) Relative leukocyte and neutrophil numbers in BAL from mice treated with pepducin or vehicle, determined by May-Grünwald-Giemsa staining 6 days after inoculation. Data represent the means ± SEM from 6 individual mice per group. (E, F) Total proteins and levels of cytokines were determined by ELISA in the BAL of infected mice (A/PR/8/34, 250 pfu/mouse, LD_{50}) after treatment with pepducin or vehicle, on day 6 post-inoculation. The results represent the means ± SEM of 6 mice per group. (G) Histopathological analysis of lungs from mice infected with A/PR/8/34 virus (250 pfu/mouse, LD_{50}) after treatment with pepducin or vehicle, on day 6 post-infection. Lung sections were stained with hematoxylin and eosin (HE). Immunohistochemistry using antibodies against Ly6G, viral NP was used to detect neutrophils and virus-infected cells. Data are representative of three mice per group. (B-F). * $p<0.05$, ** $p<0.01$ for pepducin vs. saline.

Figure 7: Eptifibatide protects mice against IAV infection, independently of the strain. (A) Ultrastructural analysis of platelets in the lungs of infected mice (A/PR/8/34, 250 pfu/mouse, LD_{50}), treated or not with eptifibatide, was performed by transmission electron microscopy. Note the aggregation of platelets in the lungs of infected mice, and their disaggregation after treatment of mice with eptifibatide. Sections show platelet aggregates with an interstitial localization. (B) Thromboxane B2 (TXB2) was measured by ELISA in the BAL of infected mice (A/NL/602/09, 30,000 pfu/mouse LD_{50}) after treatment with eptifibatide or vehicle. The results represent the means ± SEM of 3-5 mice per group. sP-selectin was measured by ELISA in the plasma of A/PR/8/34 virus-infected mice (250 pfu/mouse, LD_{50}) that were treated or not with eptifibatide, on day 6 post-inoculation. Data represent the means ± SEM of 4 mice per group. * $p<0.05$ for pepducin vs. saline. (C) Survival of mice treated with eptifibatide or vehicle after infection with IAV A/PR/8/34 (n=13 mice per group, 250 pfu/mouse), A/NL/602/09 (n=9-12 mice per group, 30,000 pfu/mouse) or A/HK/1/68 (n=12 mice per group, 100 pfu/mouse) at their respective LD_{50} values. A/FPV/Bratislava/79 was used at 5 Pfu/mouse (n=6-7 mice per group). * $p<0.05$, ** $p<0.01$ for pepducin vs. saline.

Figure 8: Eptifibatide treatment prevents severe inflammation during influenza virus infections. (A) Survival of $GPIIIa^{-/-}$ (n=5 mice/group) and WT mice (n=12 mice/group) after infection with IAV A/PR/8/34 (300 pfu/mouse) and treatment or no treatment with eptifibatide. * $p<0.05$ for eptifibatide vs. saline. (B) Lung virus titers after infection of mice with the A/NL/602/09 virus (30,000 pfu/mouse, LD_{50}) treated with eptifibatide or vehicle. Data represent the means ± SEM from 3 individual animals per group. (C) IFN-α was measured by ELISA in the BAL of infected mice (A/PR/8/34, 250 pfu/mice) after treatment

with eptifibatide or vehicle. The results represent the means ± SEM of 4 mice per group. (D, E) Total proteins and levels of cytokines were determined by ELISA in the BAL of infected mice (30 000 pfu/mouse, A/NL/602/09, LD_{50}) after treatment with eptifibatide or vehicle. The results represent the means ± SEM of 3-5 mice per group. * $p<0.05$, ** $p<0.01$ for eptifibatide vs. saline. (F) Histopathological analysis of lungs from mice infected with A/NL/602/09 virus (30 000 pfu/mouse, LD_{50}) after treatment with eptifibatide or vehicle, on day 6 post-infection. Lung sections were stained with hematoxylin and eosin (HE). Immunohistochemistry using antibodies against Ly6G and viral NP was used to detect neutrophils and virus-infected cells. Data are representative of three mice per group. (G) Survival of mice treated with MRS 2179, clopidogrel or vehicle after infection with IAV A/PR/8/34 (250 pfu/mouse; n=12 mice per group). ** $p<0.01$ for MRS 2179 vs. saline; * $p<0.05$ for clopidogrel vs. saline.

Figure 9: Histopathological analysis of lungs from infected mice after treatment with eptifibatide. (A) Histopathological analysis of lungs obtained from mice inoculated with A/PR/8/34 virus (250 PFU/mouse) and treated or not with eptifibatide. In the infected group, note the extended areas with interstitial and peribronchial inflammation and interstitial and alveolar hemorrhage. In the infected group treated with eptifibatide, note the limited areas with slight peribronchial inflammation but no major hemorrhage. (B) Blinded semiquantitative scoring of inflammatory infiltration, vascular congestion, hemorrhage, fibrin deposits and epithelial cell apoptosis in the lungs of infected mice treated or not with eptifibatide. All lung fields were examined (50x) for each sample. The scoring was performed as follows: 0=no lesion, x=mild, xx=moderate, xxx=severe.

Figure 1

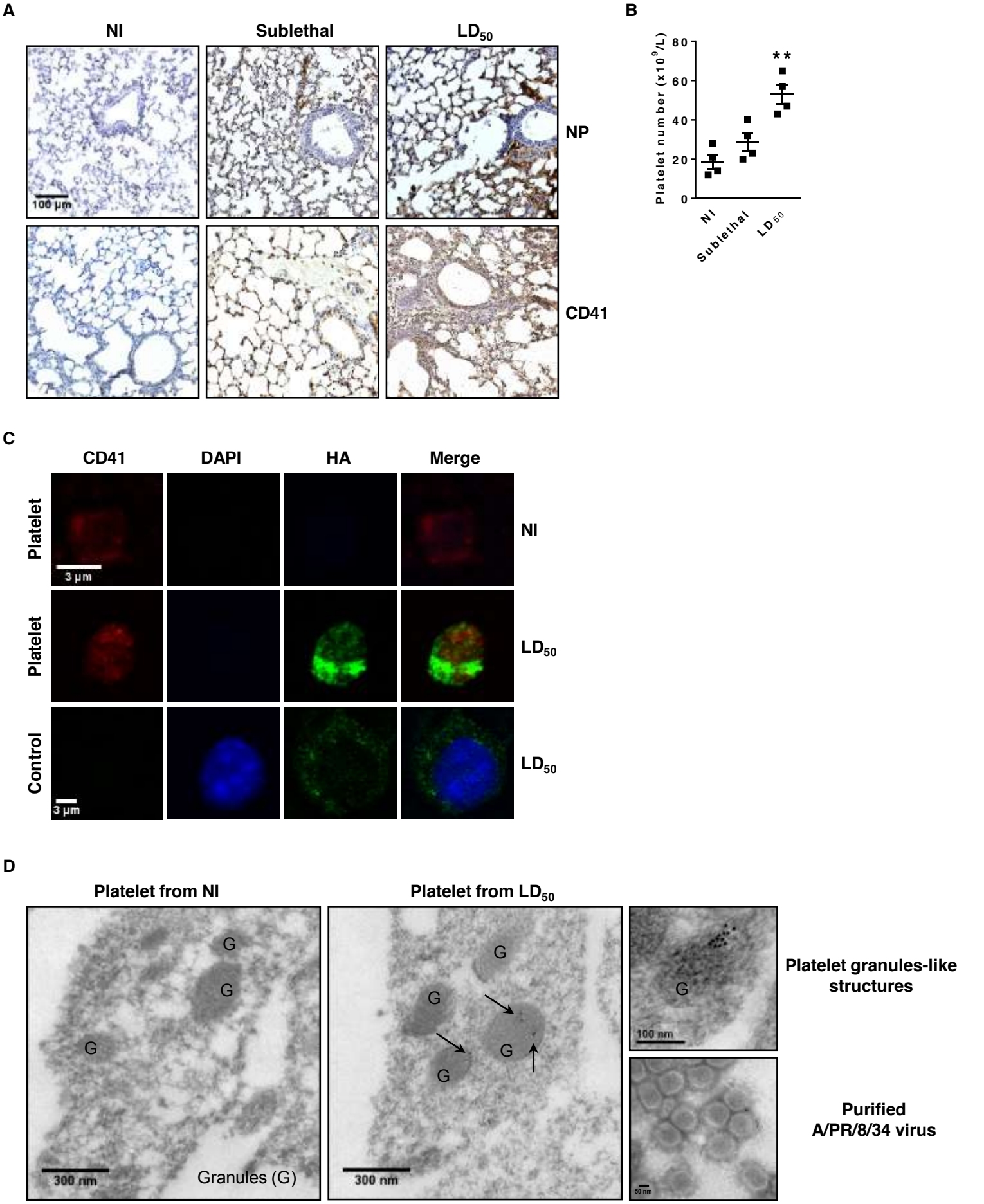
A
NI
Sublethal
LD50
NP
CD41
100 µm
B
Platelet number (x10^9/L)
80
60
40
20
0
**
NI
Sublethal
LD50
C
CD41
DAPI
HA
Merge
Platelet
Platelet
Control
NI
LD50
LD50
3 µm
3 µm
D
Platelet from NI
Platelet from LD50
G
300 nm
Granules (G)
100 nm
50 nm
Platelet granules-like structures
Purified A/PR/8/34 virus

Figure 2

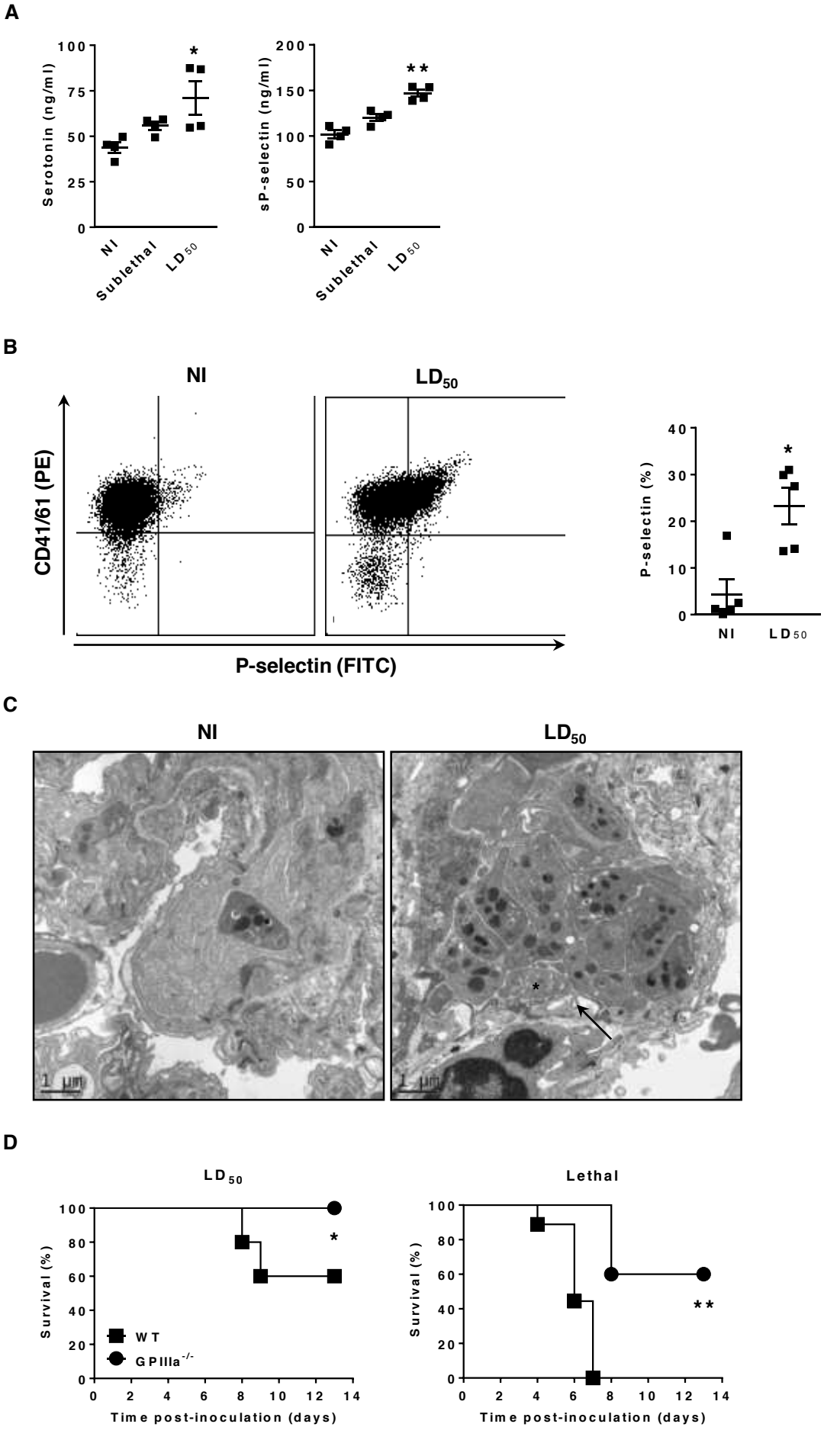
A
Serotonin (ng/ml)
sP-selectin (ng/ml)
NI
Sublethal
LD50
B
NI
LD50
CD41/61 (PE)
P-selectin (FITC)
P-selectin (%)
C
NI
LD50
D
LD50
Lethal
Survival (%)
WT
GPIIIa-/-
Time post-inoculation (days)

Figure 3

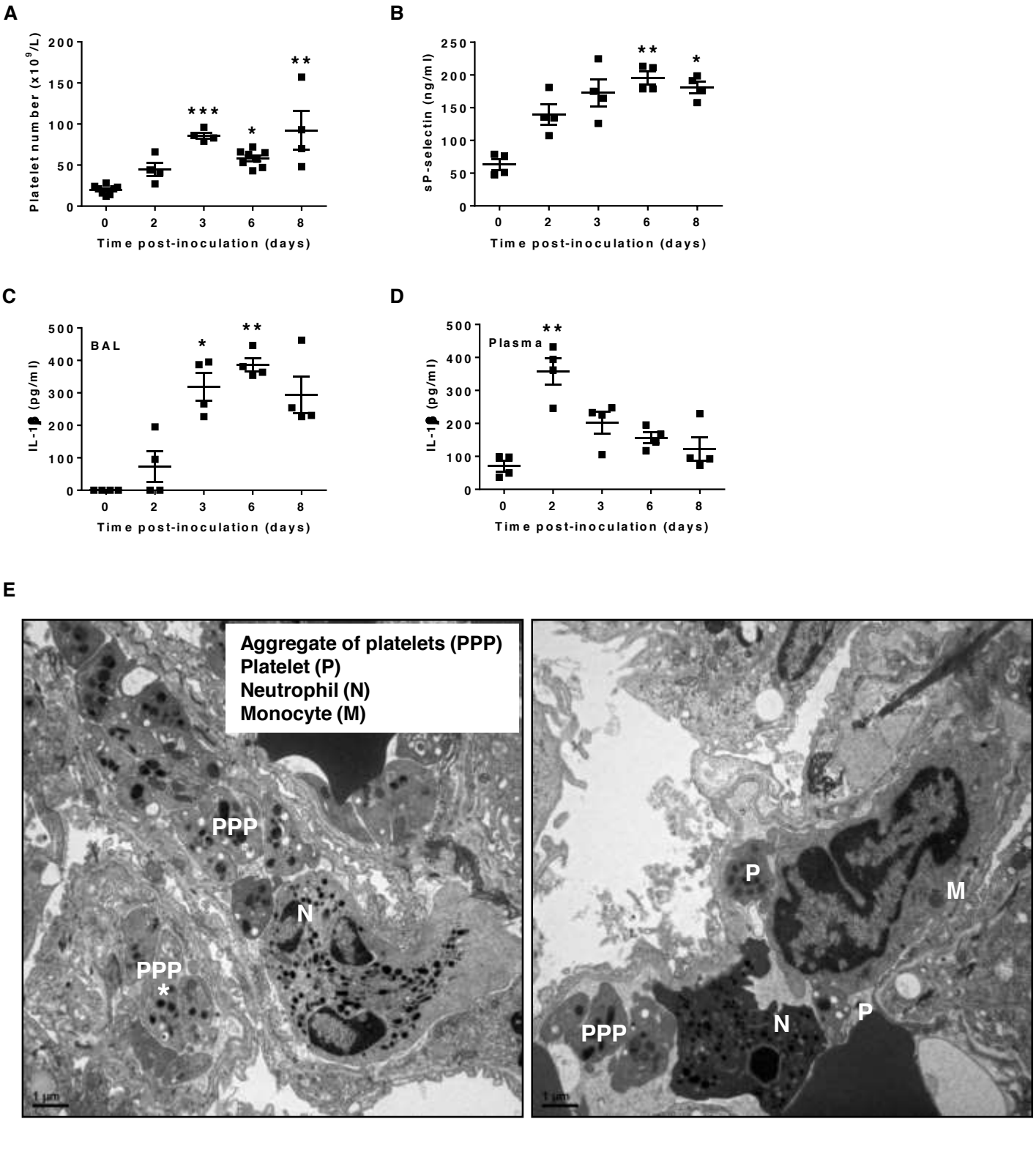
A
Platelet number (x10^9/L)
Time post-inoculation (days)
B
sP-selectin (ng/ml)
Time post-inoculation (days)
C
BAL
IL-1β (pg/ml)
Time post-inoculation (days)
D
Plasma
IL-1β (pg/ml)
Time post-inoculation (days)
E
Aggregate of platelets (PPP)
Platelet (P)
Neutrophil (N)
Monocyte (M)
PPP
N
PPP
*
1 µm
P
M
N
P
PPP
1 µm

Figure 4

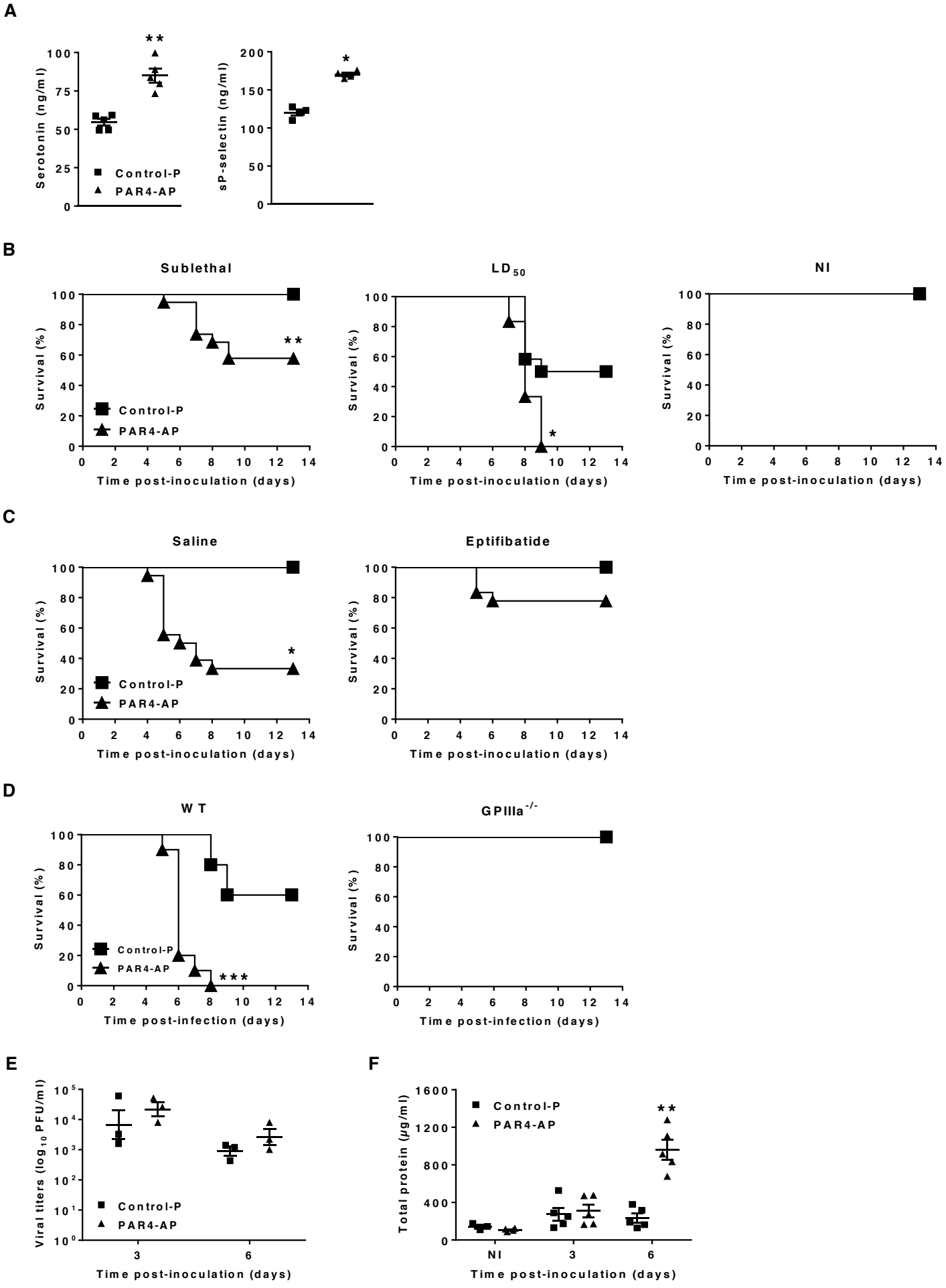
A
Serotonin (ng/ml)
sP-selectin (ng/ml)
Control-P
PAR4-AP
B
Sublethal
LD50
NI
Survival (%)
Time post-inoculation (days)
C
Saline
Eptifibatide
D
WT
GPIIIa-/-
Time post-infection (days)
E
Viral titers (log10 PFU/ml)
F
Total protein (µg/ml)

Figure 5

A

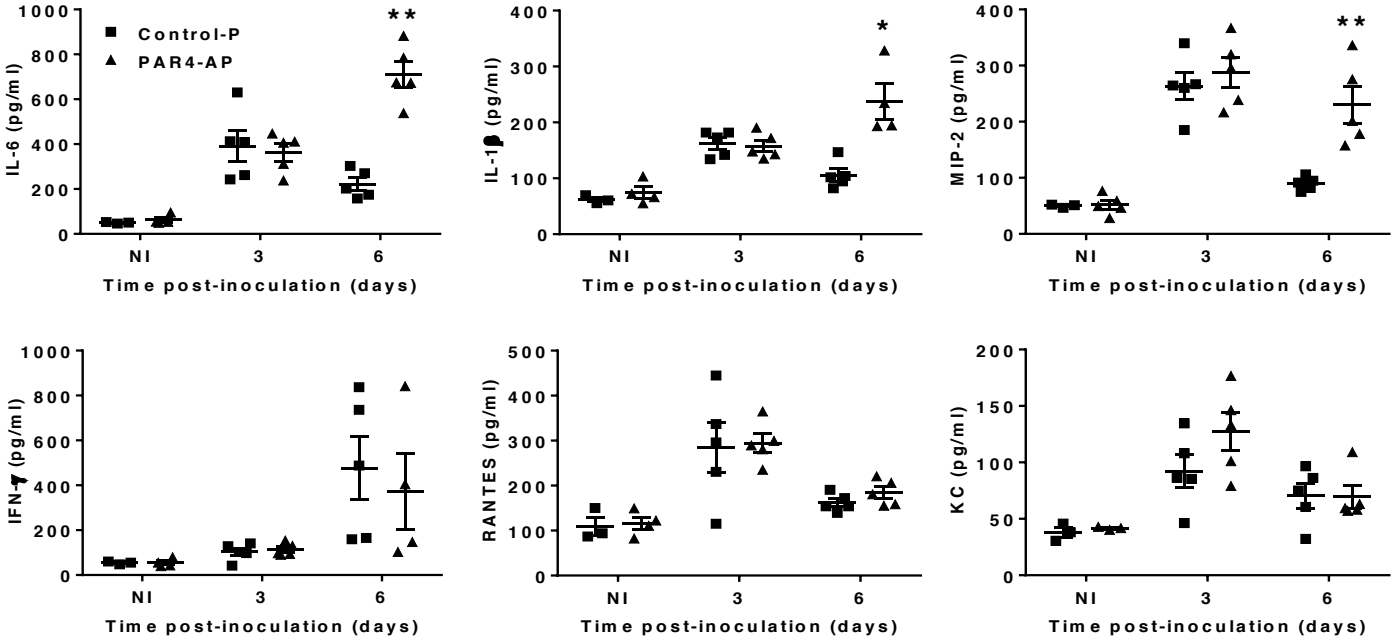
Control-P
PAR4-AP
IL-6 (pg/ml)
IL-1β (pg/ml)
MIP-2 (pg/ml)
IFN-γ (pg/ml)
RANTES (pg/ml)
KC (pg/ml)
NI
3
6
Time post-inoculation (days)
*
**

B

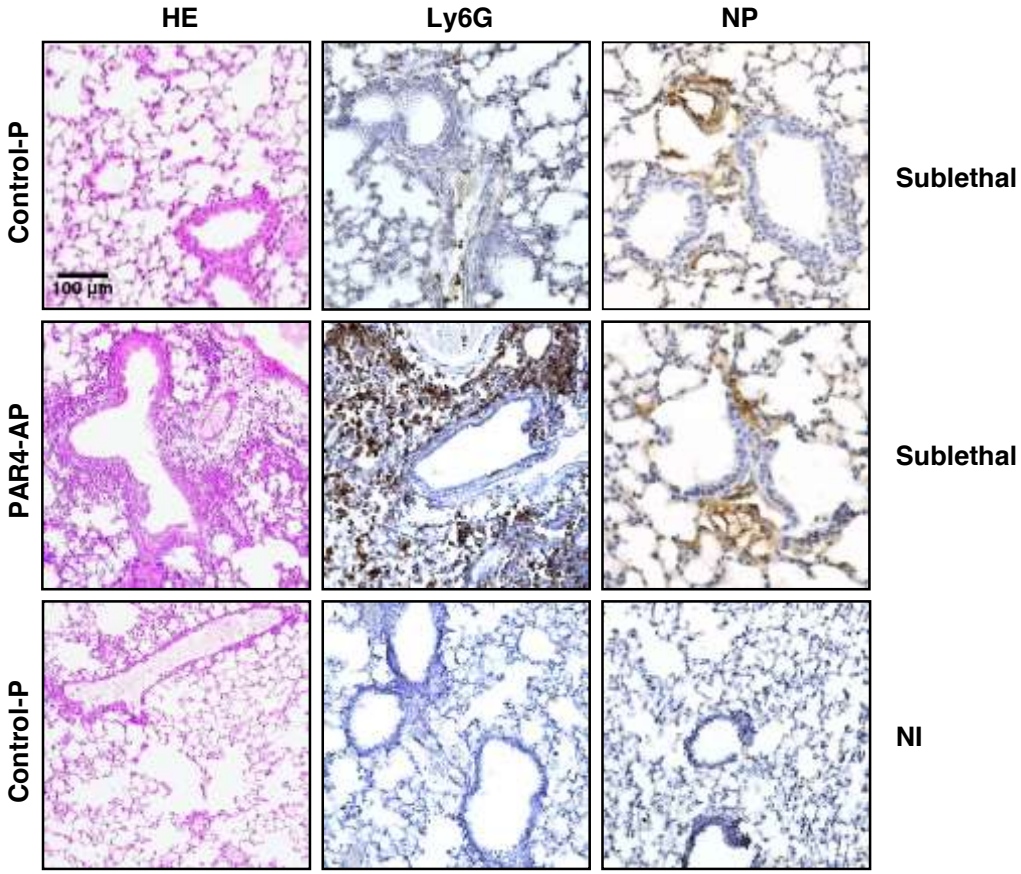
HE
Ly6G
NP
Control-P
PAR4-AP
Control-P
100 µm
Sublethal
Sublethal
NI

Figure 6

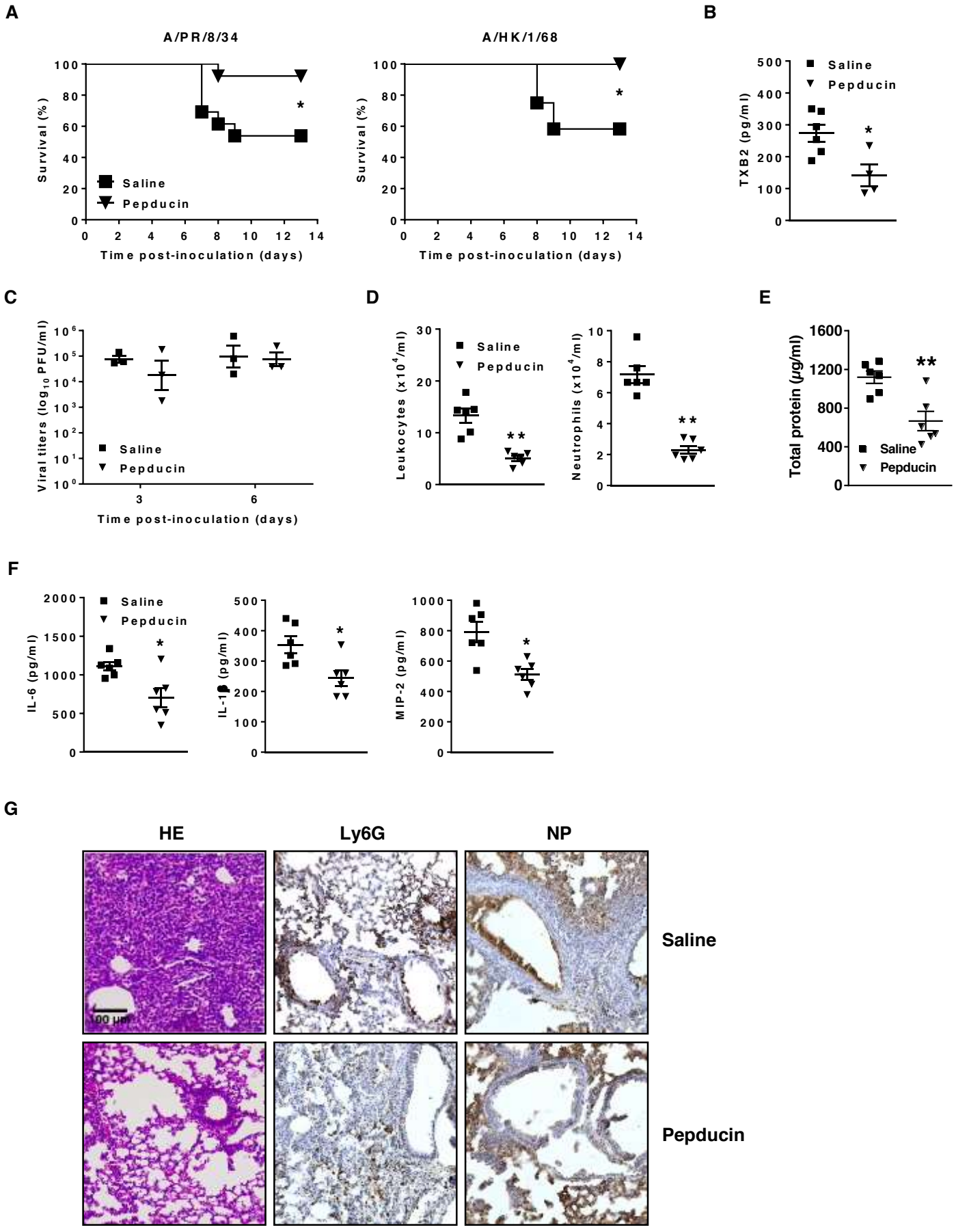
A
A/PR/8/34
A/HK/1/68
Survival (%)
Saline
Pepducin
Time post-inoculation (days)
B
TXB2 (pg/ml)
C
Viral titers (log10 PFU/ml)
D
Leukocytes (x10^4/ml)
Neutrophils (x10^4/ml)
E
Total protein (μg/ml)
F
IL-6 (pg/ml)
IL-1β (pg/ml)
MIP-2 (pg/ml)
G
HE
Ly6G
NP
100 μm
Saline
Pepducin

Figure 7

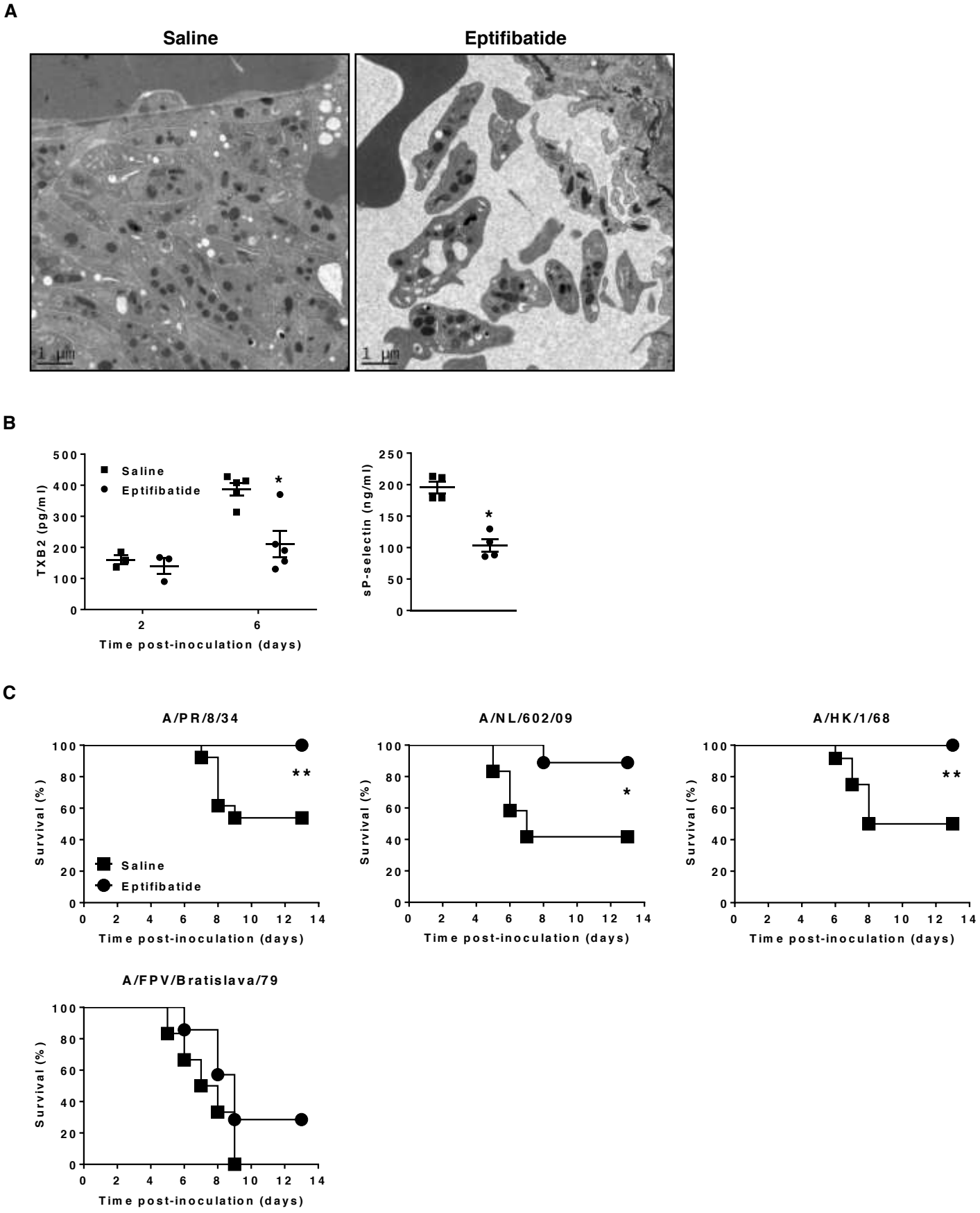
A
Saline
Eptifibatide
1 μm
1 μm
B
TXB2 (pg/ml)
Saline
Eptifibatide
*
Time post-inoculation (days)
sP-selectin (ng/ml)
*
C
A/PR/8/34
**
Survival (%)
Saline
Eptifibatide
Time post-inoculation (days)
A/NL/602/09
*
Survival (%)
Time post-inoculation (days)
A/HK/1/68
**
Survival (%)
Time post-inoculation (days)
A/FPV/Bratislava/79
Survival (%)
Time post-inoculation (days)

Figure 8

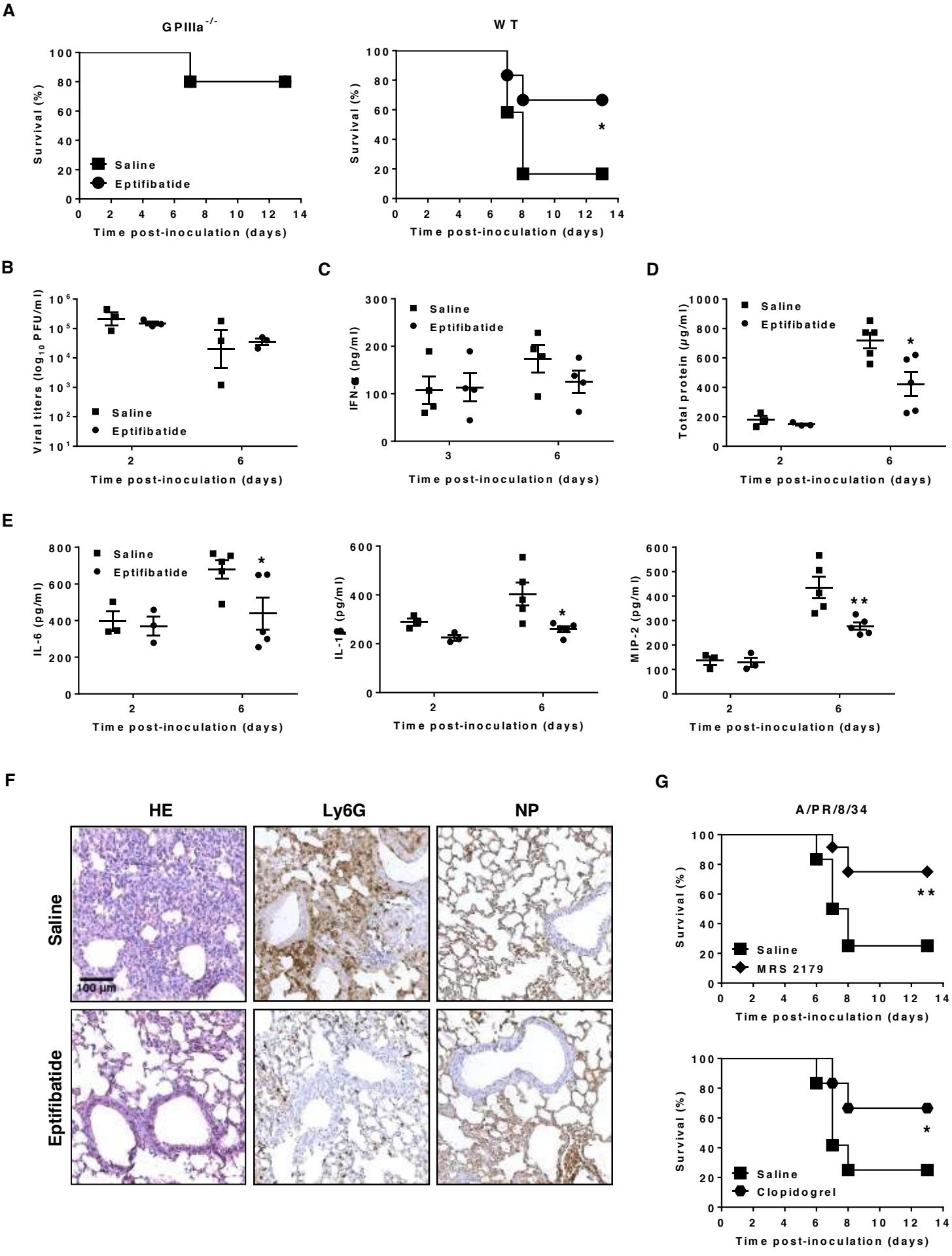
A
GPIIIa-/-
WT
Survival (%)
Saline
Eptifibatide
Time post-inoculation (days)
B
Viral titers (log10 PFU/ml)
C
IFN-γ (pg/ml)
D
Total protein (μg/ml)
E
IL-6 (pg/ml)
IL-1β (pg/ml)
MIP-2 (pg/ml)
F
HE
Ly6G
NP
Saline
Eptifibatide
100 μm
G
A/PR/8/34
MRS 2179
Clopidogrel

Figure 9

A

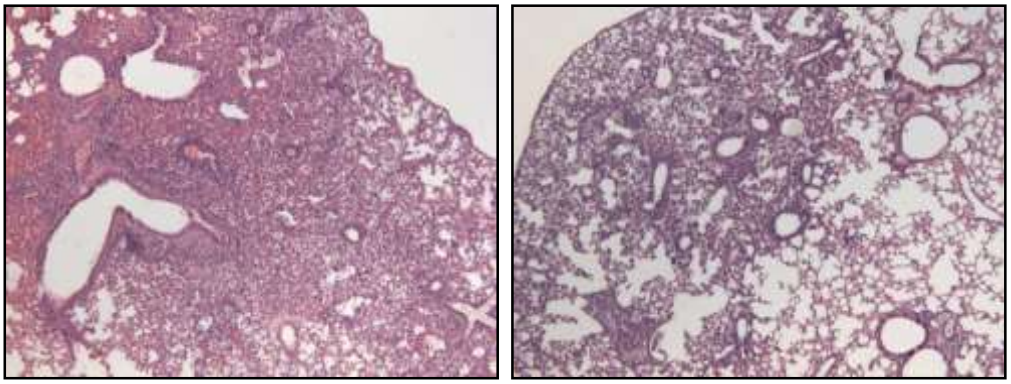

B

		Saline			Eptifibatide		
	Mouse	**1**	**2**	**3**	**1**	**2**	**3**
Neutrophil infiltration	Alveoli	++	+	+	+	+	+
	Bronchiole	++	+	+	+	+	+
	Bronchus	++	+	+	+	+	+
	Interalveolar septa	++	++	++	+	+	+
	Peribronchiolar parenchyma	++	++	++	+	+	+
	Big vessels	-	-	-	-	-	-
	Serosa	-	-	-	-	-	-
Mononuclear cell infiltration	Alveoli	+++	+++	+++	++	++	++
	Bronchiole	+++	+++	+++	++	++	++
	Bronchus	+++	+++	+++	++	++	++
	Interalveolar septa	+++	+++	+++	++	++	++
	Peribronchiolar parenchyma	+++	+++	+++	+++	+++	+++
	Big vessels	-	-	-	-	-	-
	Serosa	-	-	-	-	-	-
Vascular congestion	Alveoli	+++	++	++	-	-	+
	Bronchiole	+++	++	++	-	-	++
	Bronchus	+++	++	++	-	-	++
	Interalveolar septa	+++	++	++	-	-	++
	Peribronchiolar parenchyma	+++	++	++	-	-	++
	Big vessels	+++	++	++	+	+	++
	Serosa	+++	++	++	-	-	-
Hemorrhage	Alveoli	++	++	+	-	-	+
	Bronchiole	+	+	+	-	-	-
	Bronchus	-	-	-	-	-	-
	Interalveolar septa	-	-	-	-	-	-
	Peribronchiolar parenchyma	-	-	-	-	-	-
	Big vessels	-	-	-	-	-	-
	Serosa	-	-	-	-	-	-
Fibrin deposit	Alveoli	+++	++	++	-	-	-
	Bronchiole	-	-	-	-	-	-
	Bronchus	-	-	-	-	-	-
	Interalveolar septa	-	-	-	-	-	-
	Peribronchiolar parenchyma	-	-	-	-	-	-
	Big vessels	-	-	-	-	-	-
	Serosa	-	-	-	-	-	-
Epithelial cell apoptosis	Alveoli	++	++	++	-	-	+
	Bronchiole	++	++	++	-	-	-
	Bronchus	++	++	++	+	+	+
	Interalveolar septa	-	-	-	-	-	-
	Peribronchiolar parenchyma	-	-	-	-	-	-
	Big vessels	-	-	-	-	-	-
	Serosa	-	-	-	-	-	-